Regular Article

Large elastocaloric effect at small transformation strain in $Ni_{45}Mn_{44}Sn_{11}$ metamagnetic shape memory alloys

Wen Sun, Jian Liu *, Binfeng Lu, Yang Li, Aru Yan

Key Laboratory of Magnetic Materials and Devices, Ningbo Institute of Material Technology and Engineering, CAS, Ningbo 315201, People's Republic of China
Zhejiang Province Key Laboratory of Magnetic Materials and Application Technology, Ningbo Institute of Material Technology and Engineering, CAS, Ningbo 315201, People's Republic of China

ARTICLE INFO

Keywords:
Shape memory alloy
Martensitic phase transformation
Elastocaloric effect

ABSTRACT

The elastocaloric effect has been investigated by directly measuring temperature change in $Ni_{45}Mn_{44}Sn_{11}$ metamagnetic shape memory alloys. The stress plateau for magnetostructural transition can be drastically reduced due to the mechanical training effect. A large temperature change of 4 K was found during compressing the sample with a small transformation strain of 1.3% at 291.5 K. Our results indicate that Ni–Mn–Sn alloys can be a promising candidate for solid-state refrigerants in mechanical cooling application by low deformation level.

Elastocaloric refrigeration technology has increasingly acquired attention because of its eco-friendliness, high coefficient of performance (COP) and moderate projected cost [1–4]. Elastocaloric effect systems have been designed based on the reversible martensitic transformation (MT) accompanied by a large latent heat release/absorption [2–4]. Recently, elastocaloric cooling technique has been found to have a higher COP than the magnetic refrigerator (by using the benchmark Gd) with even higher efficiency at the same temperature span [5]. Temperature change (ΔT), as a crucial parameter in determining the functionalities of elastocaloric effect, have been directly measured in Cu–Zn–Al [6], Ni–Ti–(Cu)–(Co) [7–10], Fe–Pd [11,12], Ni–Fe–Ga–(Co) [13,14] and Ni–Mn–In–(Co) shape memory alloys (SMAs) [15–17]. Conventional Cu–Zn–Al polycrystalline alloys exhibit a ΔT of about 6 K [6]. Ni–Ti wire shows a ΔT of −21 K after 400 loading/unloading cycles in order to get a stabilized superelastic response [8]. However, the limited fatigue life and functional stability restricted the practical application of Ni–Ti alloys [7–8]. In this context, a novel Ni–Ti–Cu–(Co) alloy composition has been proposed with a rather high cyclic stability and ultra-low fatigue property due to the presence of Ti_2Cu precipitates [10]. Different from conventional SMAs, Ni–Mn-based alloys exhibit coupled magnetostructural transitions which can be driven by different stimuli [17–19]. Such multi-caloric effect enables a broadened work temperature window of magnetic refrigerants by simultaneously applying magnetic field and pressure [19,20]. For the Ni–Mn–Sn–(Co) alloys, large entropy change ($\Delta S = 40$ J / kg K) associated with MT can be obtained [21]. Therefore, a large elastocaloric effect is expected in this Heusler-type system. The elastocaloric effect in SMAs with first-order transition generally consists of different contributions from electronic, vibrational, magnetic and frictional heat parts [15]. For the $Ni_{45}Mn_{44}Sn_{11}$ alloy, the austenitic phase shows a ferromagnetic–paramagnetic transition in a magnetic field during cooling [22]. As the Curie temperature (T_C^A) of austenitic phase and the austenite transformation finish temperature (A_f) near to each other, the difference in magnetic moments for both parent and martensite phases around structural transition temperature is small and the negative contribution of magnetic entropy is limited. This is beneficial for achieving large elastocaloric effect. In this work, the elastocaloric effect of the mechanically trained sample was investigated by directly measuring ΔT. We also address the impact of strain rate on ΔT during loading/unloading cycles.

A polycrystalline $Ni_{45}Mn_{44}Sn_{11}$ ingot was arc-melted and then sucked into a 3 mm diameter copper mold via a pressure difference in argon atmosphere. Suction casting generally results in a grain refinement effect that is able to improve the mechanical properties of the alloy [23]. Cylinder samples with 3 mm in diameter and 5.8 mm in length for mechanical tests were cut from the rod-like alloy, and then homogenized at 1173 K for 24 h in argon atmosphere, followed by quenching into ice water. MT temperatures and transformation enthalpies were characterized by a differential scanning calorimeter (PerkinElmer Diamond DSC) with cooling and heating rates of 10 K/min. Compression experiments were conducted on a universal testing machine (SUNS UTM5000) at room temperature. The strain was measured by an extensometer. The temperature changes of sample under different strain rates were monitored by a K-type thermocouple pasted on the sample surface.

* Corresponding author at: J. Liu, Key Laboratory of Magnetic Materials and Devices, Ningbo Institute of Material Technology and Engineering, CAS, Ningbo 315201, People's Republic of China.
E-mail address: liujian@nimte.ac.cn (J. Liu).

Fig. 1(a) shows the characteristic transformation temperatures detected by DSC. The MT starts (M_s) at 266.6 K and finishes (M_f) at 257.1 K, and austenite transformation starts (A_s) at 269.3 K and A_f at 279.5 K. A small transition peak represents the Curie temperature of T_C^A at 286 K as shown in the inset of Fig. 1(a). Transformation enthalpy (ΔH) is calculated to be −8.4 J/g for cooling and 9.3 J/g for heating. Entropy change in thermal-induced MT can be determined by $\Delta S = \Delta H / T_0$, where T_0 is the equilibrium temperature defined as $(M_s + A_f) / 2$ [13]. ΔS is calculated to be −30.8 J/kg K for cooling and 34.1 J/kg K for heating. Theoretical ΔT caused by the entropy change during thermal-induced MT can be estimated through $\Delta T = -(\Delta S \times T) / C_p$ [14], where C_p is the heat capacity (taken as 583 J/kg K) [24]. The calculated $\Delta T = -15.4$ K for cooling and 17.1 K for heating from DSC measurements. At T = 291.5 K (12 K above A_f), various maximum compressive stresses (σ) were applied at a strain rate of 0.023% s^{-1} as shown in Fig. 1(b). An initial plateau appeared in the stress–strain curve when σ is 250 MPa, typically indicating the stress-induced MT. The transformation strain (ε^T) increases with increasing σ during loading. Meanwhile, the critical stress is significantly reduced. The ε^T is 2.3%, and critical stress is 172 MPa when σ is 290 MPa. In order to stabilize the critical stress, the sample was initially trained by cyclic loading/unloading before measuring elastocaloric effects.

Fig. 2(a) shows the training impact during mechanical cycling in $Ni_{45}Mn_{44}Sn_{11}$ alloys. The compressive stress of 260 MPa was applied at a strain rate of 0.029% s^{-1}. The sample was subjected to 6 loading/unloading cycles. The critical stress decreases from 250 to 178.6 MPa due to mechanical training, as shown in Fig. 2(b). The reduction of critical stress is most pronounced during the 2nd loading/unloading cycle. The value of ε^T increases from 0.3 to 1.1% during mechanical cycles. The principle of the training method is that deforming the parent or martensite phase creates sites of internal stress, or simultaneously forms precipitates [25]. The decrease of critical stress may be due to

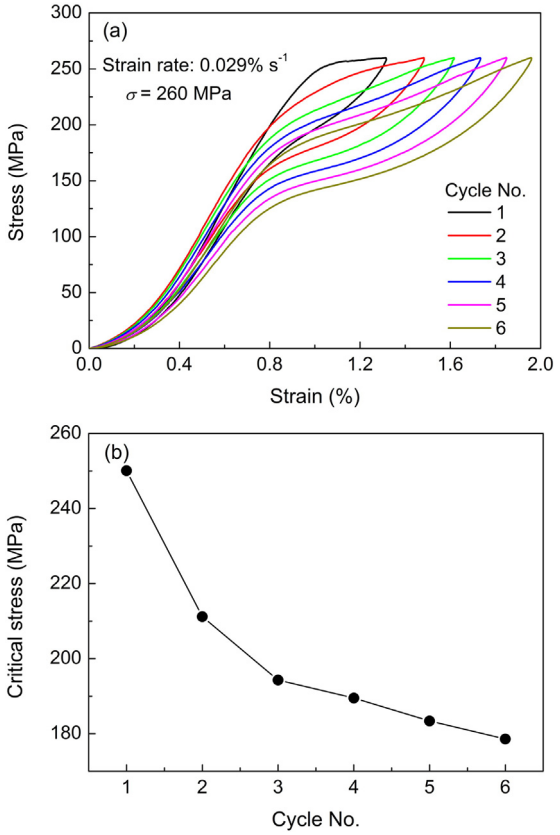

Fig. 2. Superelastic training at 291.5 K with the strain rate of 0.029% s^{-1} (a) and evolution of the critical transformation stress as a function of the cycle number (b).

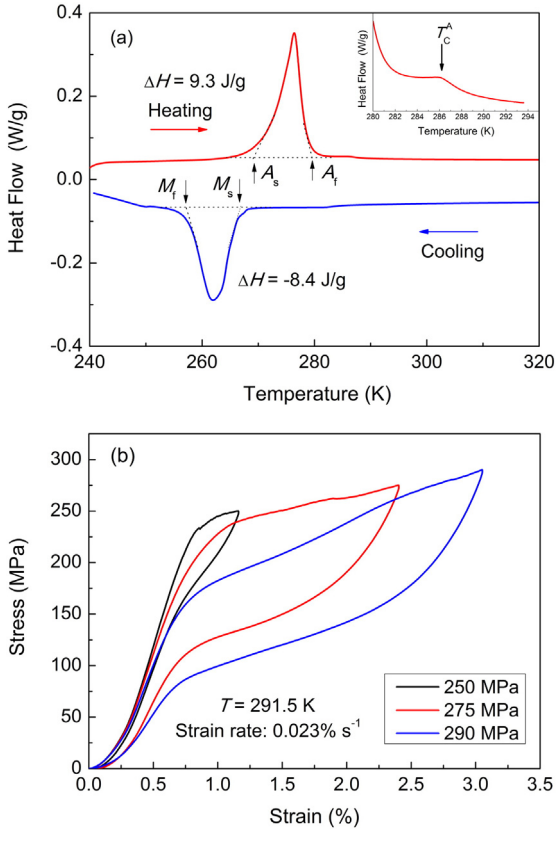

Fig. 1. DSC curve (a) and stress–strain responses for various applied maximum compressive stresses at a low strain rate of 0.023% s^{-1} (b) in annealed $Ni_{45}Mn_{44}Sn_{11}$ alloy.

the presence of dislocation induced by deformation in $Ni_{45}Mn_{44}Sn_{11}$ alloys. The internal stress formed by dislocation assists the formation of the stress-induced martensite during loading in the subsequent cycles [8,25].

Fig. 3(a) shows the stress–strain curves at high strain rates for the mechanically trained sample. In order to avoid the crack in the Ni–Mn–Sn cylinder sample, the maximum applied stress is constrained to be 242 MPa. After the first loading from 0 to 242 MPa, the stress was held for 30 s to allow the sample to reach equilibrium condition and unloaded to zero at the same strain rate. The stress–strain responses approach a stable level during loading when the strain rate is less than 0.57% s^{-1}. However, the sample fractured during the stress holding step in the case of fast loading at 0.85% s^{-1}. The fast loading is prone to produce micro-cracks which propagate and eventually damage the sample during stress holding. Therefore, the appropriate strain rate should be less than 0.57% s^{-1} to maintain a stable superelasticity. The ε^T increases with increasing strain rate during loading/unloading cycles to approach a complete martensitic transformation. The strain vs. time curve is simultaneously monitored, as shown in Fig. 3(b). The fast loading shortens the time to achieve the target stress. The time interval for loading the sample from 0 to 242 MPa is only 3 s at a strain rate of 0.85% s^{-1}. The ΔT-time profiles at different strain rates are shown in Fig. 3(c). The increased strain rate leads to a better adiabatic environment and larger ε^T. The temperature change during loading ($\Delta T_{loading}$) of 4 K was observed at the strain rate of 0.85% s^{-1}. Such a large temperature change, on the one hand, essentially originates from the large latent heat of stress-induced martensitic transition and the relatively small magnetization difference between austenitic and martensitic phases, as mentioned in the introduction part. On the other hand, one should notice that the testing temperature is close to the T_C^A. Around the second order transition temperature (T_C^A) in Heusler-type alloys, for instance $Ni_{45}Co_5Mn_{36.6}In_{13.4}$, a strong magnetoelastic coupling can

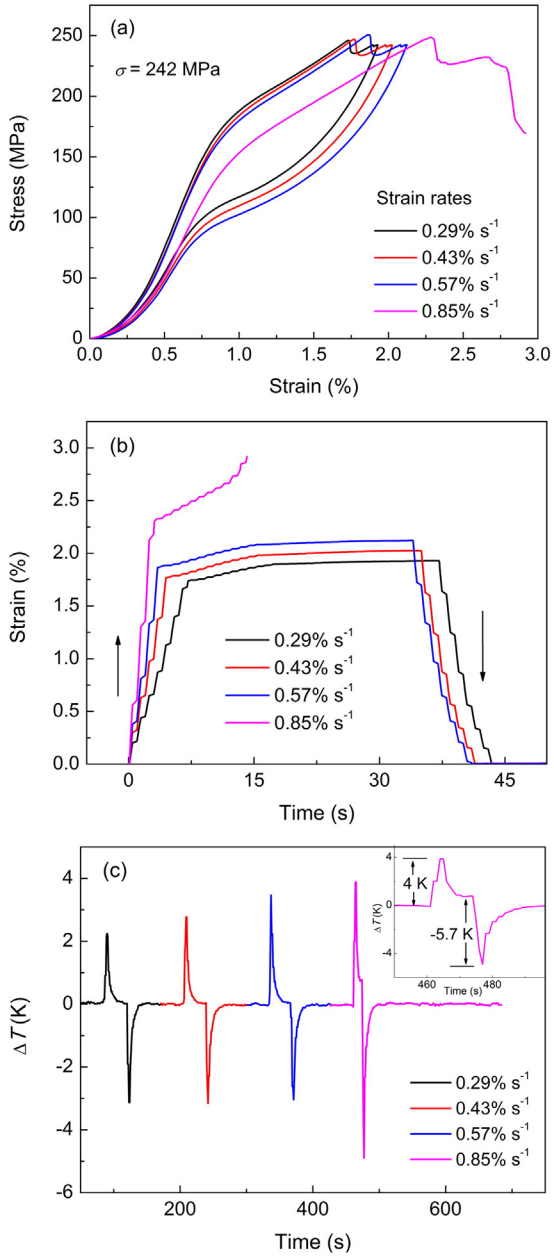

Fig. 3. Stress–strain curves (a) and strain vs. time curves (b) in high strain rates for the mechanically trained sample. Temperature changes at different strain rates during loading/unloading and the enlarged profile (inset) at the strain rate of 0.85% s^{-1} (c).

take place, where the lattice entropy (phonon softening) and the magnetic entropy (elongation and spin ordering of magnetic moment) contribute with the same sign to the total entropy change [26]. As a consequence, an apparent magnetically induced adiabatic temperature change was observed (2 K at 1.9 T) [27]. Therefore, the present observed large elastocaloric effect, even at small transformation strains, can also be ascribed to an additional entropy change from giant magneto-elasticity by crossing T_C^A.

Next we discuss the strain rate dependent elastocaloric effect. At a strain rate of 0.29% s^{-1}, the absolute value of temperature change during unloading ($|\Delta T_{unloading}|$) of about 3 K is higher than $|\Delta T_{loading}|$ (2 K). This phenomenon is attributed to a larger ε^T during unloading compared with loading. In addition, we found that the absolute value of $|\Delta T_{unloading}|$ (about 3 K) is smaller than $|\Delta T_{loading}|$ (about 3.5 K) at strain rate of 0.57% s^{-1}. Due to the martensitic and austenitic phase boundary movement in both loading and unloading procedures, the resulting friction effect is always accompanied by the heat release [15]. Upon loading, the increased ε^T and frictional heat contribute the same sign to the $\Delta T_{loading}$, but latent heat and friction heat somehow counteract each other on unloading, therefore the $\Delta T_{unloading}$ seems unchanged with increasing strain rate. When the strain rate is applied up to 0.85% s^{-1}, the compression force is released suddenly due to the sample fracture. Nevertheless, we have observed a large $\Delta T_{unloading}$ of −5.7 K at 0.85% s^{-1}, as shown in the inset of Fig. 3(c). The measured $|\Delta T|$ is far less than the calculated value (15.4 K) from the DSC measurement. The small measured value is due to incomplete martensite transformations and non-ideal adiabatic conditions.

A systematic comparison of elastocaloric performance between Ni–Mn–Sn and other magnetic SMAs is shown in Table 1. In this work, the specific elastocaloric cooling strength ($|\Delta T / \sigma|$) reaches about 23.6 K/GPa in $Ni_{45}Mn_{44}Sn_{11}$ SMAs. The $\Delta T_{loading}$ at transformation strain of 1% ($|\Delta T_{loading} / \Delta\varepsilon^T|$) is about 3.1 K/1%. Compared with other metamagnetic SMAs such as Ni–Mn–In and Ni–Mn–In–Co metamagnetic SMAs [16,17], the present $Ni_{45}Mn_{44}Sn_{11}$ alloy shows larger elastocaloric effect (−5.7 K). As compared with Fe–Pd, Ni–Fe–Ga and Ni–Fe–Ga–Co SMAs [11,13,14], the advantages of Ni–Mn–Sn alloys with metamagnetic transition properties exhibit higher elastocaloric effects at low ε^T. It has been reported that applying smaller strains can increase the fatigue life, at the same time keeping a reasonably elastocaloric effect and cooling power of refrigerant device [2,5]. Nevertheless, Ni–Mn–Sn alloys are intrinsically brittle in its polycrystalline state, which restrict their practical applications. The introduction of secondary ductile phases [13] and the texturing formation in directionally solidified alloys [28] could be considered to partially solve the mechanical obstacles in Ni–Mn–Sn alloys.

In conclusion, mechanical training has been demonstrated as a feasible way to reduce the transformation stress and achieve a large temperature change by small transformation strain (3.1 K / 1%) in $Ni_{45}Mn_{44}Sn_{11}$ alloys. A stable $\Delta T_{unoading}$ of 3 K is obtained for loading/unloading cycles at the moderate strain rate (0.29%–0.57% s^{-1}). A large $\Delta T_{loading}$ of 4 K can be achieved at the strain rate of 0.85% s^{-1}.

The research leading to these results has received funding from the National Natural Science Foundation of China (Grant Nos. 51371184 and 51531008), Projects of Ningbo Innovative Research Team (Grant No. 2012B81001) and Ningbo Natural Science Foundation of China (Grant Nos. 2014A610164 and 2014A610160).

Table 1
The finishing temperature of austenite transformation (A_f), temperature change from direct measurements during unloading ($\Delta T_{unloading}$) at initial temperature (T_{ini}), strength of elastocaloric effects ($|\Delta T / \sigma|$) and elastocaloric effects at transformation strain of 1% ($\Delta T_{loading} / \Delta\varepsilon^T$) in magnetic alloys.

Alloy composition (at.%)	Sample status	A_f (K)	T_{ini} (K)	$\Delta T_{unloading}$ (K)	$\lvert\Delta T/\sigma\rvert$ (K/GPa)	$\Delta T_{loading}/\Delta\varepsilon^T$ (K/1%)	Reference
$Fe_{68.8}Pd_{31.2}$	Single crystal	239.6	240	−2	20	1.7	[11]
$Ni_{54}Fe_{19}Ga_{27}$	Polycrystal	290	300	−6	45.1	2.7	[13]
$Ni_{50}Fe_{19}Ga_{27}Co_4$	Single crystal	320	348	−10	33.3	2.1	[14]
$Ni_{45}Mn_{36.4}In_{13.6}Co_5$	Polycrystal	275	296	−4	26.7	1.3	[16]
$Ni_{48}Mn_{35}In_{17}$	Textured polycrystal	Unkown	313.3	−4	13.3	3.6	[17]
$Ni_{45}Mn_{44}Sn_{11}$	Polycrystal	279.5	291.5	−5.7	23.6	3.1	This work

References

[1] X. Moya, S. Kar-Narayan, N.D. Mathur, Nat. Mater. 13 (2014) 439–450.
[2] M. Schmidt, A. Schütze, S. Seelecke, Int. J. Refrig. 54 (2015) 88–97.
[3] S. Crossley, N.D. Mathur, X. Moya, AIP Adv. 5 (2015) 067153.
[4] L. Mañosa, A. Planes, M. Acet, J. Mater. Chem. A 1 (2013) 4925–4936.
[5] J. Tušek, K. Engelbrecht, R. Millán-Solsona, L. Mañosa, E. Vives, L.P. Mikkelsen, N. Pryds, Adv. Energy Mater. 5 (2015) 1500361.
[6] L. Mañosa, S. Jarque-Farnos, E. Vives, A. Planes, Appl. Phys. Lett. 103 (2013) 211904.
[7] J. Cui, Y.M. Wu, J. Muehlbauer, Y. Hwang, R. Radermacher, S. Fackler, M. Wuttig, I. Takeuchi, Appl. Phys. Lett. 101 (2012) 073904.
[8] J. Tušek, K. Engelbrecht, L.P. Mikkelsen, N. Pryds, J. Appl. Phys. 117 (2015) 124901.
[9] C. Bechtold, C. Chluba, R.L. de Miranda, E. Quandt, Appl. Phys. Lett. 101 (2012) 091903.
[10] C. Chluba, W. Ge, R.L. de Miranda, J. Strobel, L. Kienle, E. Quandt, M. Wuttig, Science 348 (2015) 1004.
[11] F. Xiao, T. Fukuda, T. Kakeshita, Appl. Phys. Lett. 102 (2013) 161914.
[12] F. Xiao, T. Fukuda, T. Kakeshita, X.J. Jin, Acta Mater. 87 (2015) 8–14.
[13] Y. Xu, B.F. Lu, W. Sun, A.R. Yan, J. Liu, Appl. Phys. Lett. 106 (2015) 201903.
[14] F. Xiao, M.J. Jin, J. Liu, X.J. Jin, Acta Mater. 96 (2015) 292–300.
[15] B.F. Lu, F. Xiao, A.R. Yan, J. Liu, Appl. Phys. Lett. 105 (2014) 161905.
[16] B.F. Lu, P.N. Zhang, Y. Xu, W. Sun, J. Liu, Mater. Lett. 148 (2015) 110–113.
[17] Y.J. Huang, Q.D. Hu, N.M. Bruno, J.H. Chen, I. Karaman, J.H. Ross Jr., J.G. Li, Scr. Mater. 105 (2015) 42–45.
[18] P.O. Castillo-Villa, L. Mañosa, A. Planes, D.E. Soto-Parra, J.L. Sánchez-Llamazares, H. Flores-Zúñiga, C. Frontera, J. Appl. Phys. 113 (2013) 053506.
[19] A.K. Nayak, K.G. Suresh, A.K. Nigam, A.A. Coelho, S. Gama, J. Appl. Phys. 106 (2009) 053901.
[20] S. Esakki Muthu, N.V. Rama Rao, M. Manivel Raja, S. Arumugam, K. Matsubayasi, Y. Uwatoko, J. Appl. Phys. 110 (2011) 083902.
[21] D.Y. Cong, S. Roth, L. Schultz, Acta Mater. 60 (2012) 5335–5351.
[22] Z.D. Han, D.H. Wang, C.L. Zhang, H.C. Xuan, B.X. Gu, Y.W. Du, Appl. Phys. Lett. 90 (2007) 042507.
[23] Y. Li, Y. Xin, C.B. Jiang, H.B. Xu, Scr. Mater. 51 (2004) 849–852.
[24] M. Pasquale, C.P. Sasso, L. Giudici, T. Lograsso, D. Schlagel, Appl. Phys. Lett. 91 (2007) 131904.
[25] J. Fernandez, X.M. Zhang, J.M. Guilemany, J. Mater. Process. Technol. 139 (2003) 117.
[26] P.J. Stonaha, M.E. Manley, N.M. Bruno, I. Karaman, R. Arroyave, N. Singh, D.L. Abernathy, S. Chi, Phys. Rev. B 92 (2015) 140406.
[27] J. Liu, T. Gottschall, K.P. Skokov, J.D. Moore, O. Gutfleisch, Nat. Mater. 11 (2012) 620–626.
[28] B. Yuan, P.Q. Zheng, Y. Gao, M. Zhu, D.C. Dunand, Mater. Des. 80 (2015) 28–35.